Tandem electrocatalytic N2 fixation via concerted proton-electron transfer

Jonas Peters (jonas.peters@gmail.com)
California Institute of Technology https://orcid.org/0000-0002-6610-4414
Pablo Garrido-Barros
California Institute of Technology
Joseph Derosa
California Institute of Technology
Matthew Chalkley
California Institute of Technology

Physical Sciences - Article

Keywords: electrochemical ammonia synthesis, tandem catalysis, concerted proton-electron transfer

Posted Date: November 23rd, 2021

DOI: https://doi.org/10.21203/rs.3.rs-1000646/v1

Version of Record: A version of this preprint was published at Nature on August 31st, 2022. See the published version at https://doi.org/10.1038/s41586-022-05011-6.

Title: Tandem electrocatalytic N_2 fixation via concerted proton-electron transfer

Authors: Pablo Garrido-Barros, Joseph Derosa, Matthew J. Chalkley[†] & Jonas C. Peters*

Affiliations:

Division of Chemistry and Chemical Engineering, California Institute of Technology; Pasadena, CA 91125, USA.

[†]Present address: Department of Pharmaceutical Chemistry, University of California, San Francisco, CA, USA

*Corresponding author. Email: jpeters@caltech.edu

Abstract:

New electrochemical ammonia (NH_3) synthesis technologies are of interest as a complementary route to the Haber-Bosch (HB) process for distributed fertilizer generation, and towards exploiting ammonia as a zero-carbon fuel produced via renewably-sourced electricity.[1–4] Apropos of these goals is a surge of fundamental research targeting heterogeneous materials[5–7] as electrocatalysts for the nitrogen reduction reaction (N_2RR). These systems generally suffer from poor stability and NH_3 selectivity; competitive hydrogen evolution reaction (HER) outcompetes N_2RR.[8] Molecular catalyst systems can be exquisitely tuned and offer an alternative strategy,[9] but progress has thus far been thwarted by the same selectivity issue; HER dominates. Herein we describe a tandem catalysis strategy that offers a solution to this puzzle. A molecular complex that can mediate an N_2 reduction cycle is partnered with a co-catalyst that interfaces the electrode and an acid to mediate concerted proton-electron transfer (CPET) steps, facilitating N–H bond

formation at a favorable applied potential and overall thermodynamic efficiency. Without CPET, certain intermediates of the N_2RR cycle would be unreactive via independent electron transfer (ET) or proton transfer (PT) steps, thereby shunting the system. Promisingly, complexes featuring several metals (W, Mo, Os, Fe) achieve N_2RR electrocatalysis at the same applied potential in the presence of the CPET mediator, pointing to the generality of this tandem approach.

Main Text:

In the drive to develop electrocatalytic strategies for ammonia synthesis that complement HB (Fig. 1a), molecular catalysts offer a number of distinct advantages. In particular, they can be carefully tuned to satisfy the electronic requirements of N_2 binding and activation. They can also afford access to insightful mechanistic studies at the level of critical bond-breaking and making steps. Remarkable progress has been made over the past two decades in terms of chemically driven N_2RR catalysis and mechanistic understanding using molecular systems.[9–12] Despite this, bona fide N_2RR electrocatalysis in this domain remains virtually unknown;[13–16] only one such synthetic electrocatalyst (a tris(phosphine)borane iron ((TPB)Fe) system from our lab, Fig. 1b) has been reliably demonstrated, but it requires low temperatures (−35 °C) to mitigate background HER, operates with low turnover, and requires a highly reducing potential (−2.1 V vs ferrocenium/ferrocene, $Fc^{+/0}$; all potentials herein are reported vs $Fc^{+/0}$).[17] This state of affairs sharply contrasts the substantial progress that has been made applying molecular systems towards electrocatalytic HER, the carbon dioxide reduction reaction (CO_2RR), and the oxygen reduction reaction (ORR), among other transformations.[18–21]

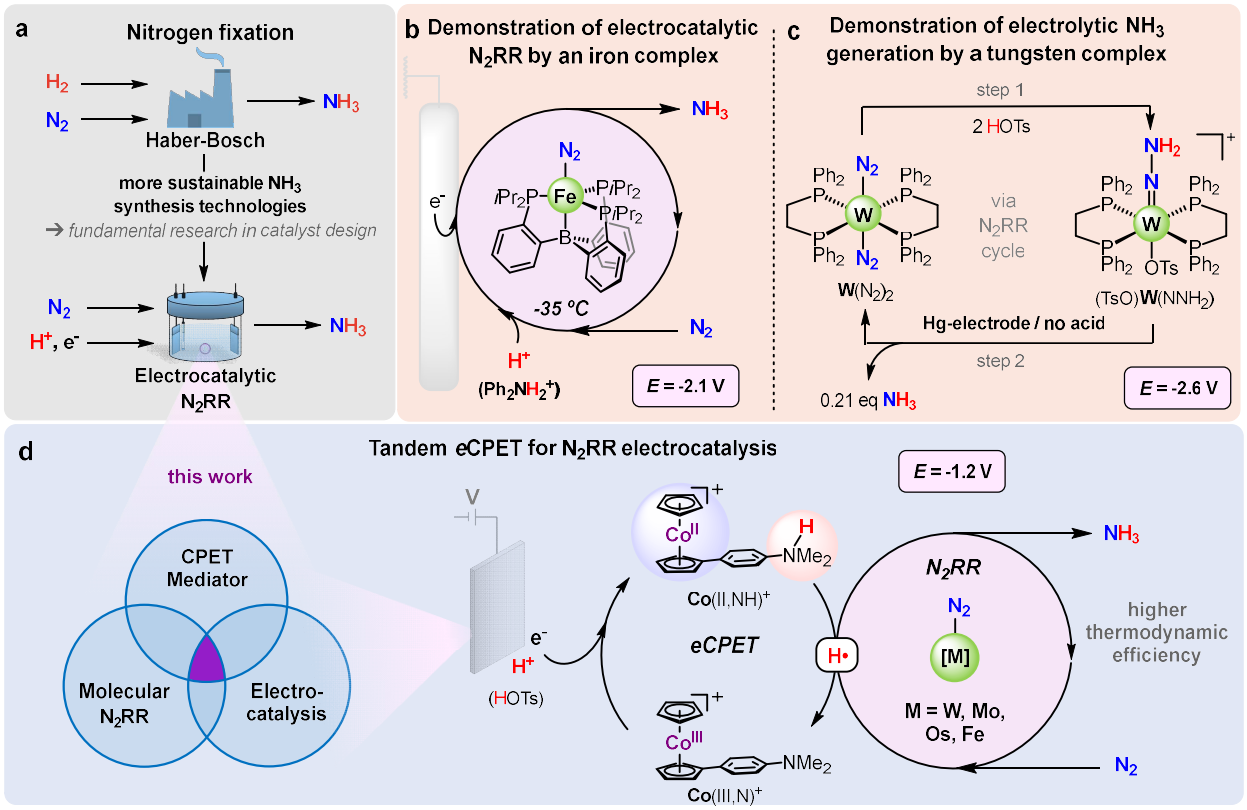

Fig. 1. Approaches to N_2RR electrocatalysis. a, Nitrogen fixation based on the traditional Haber-Bosch (HB) process versus electrochemical approaches to N_2RR that require fundamental research in catalyst design. **b**, The only molecular N_2RR electrocatalyst reported thus far based on the (TPB)Fe system operating at −2.1 V on a glassy carbon electrode using at temperature of −35ºC. **c**, Early work by Pickett demonstrating electro-synthesis of NH_3 using the molecular complex **W**$(N_2)_2$ at an applied potential of −2.6 V on a Hg-pool electrode using tosic acid (TsOH). The protonation step 2 had to be performed separately from the reduction step (0.21 equiv NH_3 / **W**$(N_2)_2$ after one cycle; 0.73 equiv total NH_3 / **W**$(N_2)_2$ after three cycles). **d**, Tandem catalysis described in this work based on coupling the CPET mediator, **Co**$(II,NH)^+$, with molecular N_2RR catalysts to enable well-defined electrocatalysis at comparatively mild potentials (−1.2 V using TsOH).

Similar to candidate heterogeneous electrocatalysts, molecular systems typically mediate HER in preference to N_2RR, and/or operate at such reducing potentials that background HER at a working electrode dominates. Pioneering research from 1985 by Pickett and coworkers underscored this point (Fig. 1c). In a study involving a bis(diphenylphosphinoethane)tungsten (abbreviated throughout as **W**) system, they showed that the hydrazido complex (TsO)**W**$(NNH_2)^+$ (TsO = tosylate), generated via protonation of the bis-N_2 adduct **W**$(N_2)_2$ by tosic acid (TsOH), releases NH_3 (0.21 equiv NH_3 per **W**) upon application of a highly reducing potential (−2.6 V on a Hg-pool electrode), but only in the absence of the acid.[22] In follow-up work, attempts to render this tungsten system electrocatalytic using various electrodes in the presence of acids led to even lower NH_3 yields (≤ 0.1 equiv NH_3 per **W**).[23] Strategies that attenuate the HER rate, for example by positively shifting the operating potential while still maintaining a significant N_2RR rate, are essential. Scaling relationships have historically frustrated such an approach; as the operating potential for reductive electrocatalysis is tuned positively, the rate of the desired transformation decreases.[24,25] Therefore, pathways to break such scaling relationships and achieve efficient electrocatalytic N_2RR at comparatively mild potentials are needed.

Recent work from our lab introduced a strategy for attenuating the rate of (electro)catalytic HER. Via the use of a concerted proton-electron transfer (CPET) mediator, comprised of cobaltocenium modified by a tethered Brønsted base (abbreviated herein as **Co**(III,N)$^+$; Fig. 1d),[26] catalyzed HER is prevented. This mediator design spatially and electronically separates the proton and electron relays, key to storing highly reactive H atom equivalents as **Co**(II,NH)$^+$ at a potential that is sufficiently mild to also mitigate background HER at the electrode. Initial model studies using this mediator established that electrochemical CPET (*e*CPET) provides a means to reduce

77 unsaturated organic substrates by applying a comparatively mild potential in the presence of tosic
78 acid.[26,27]

79 While these results point to the possibility of applying such a mediator towards
80 electrocatalytic N_2RR, the mediator itself does not react with N_2, in contrast to unsaturated organic
81 substrates. Hence, we have pursued a tandem catalysis strategy (Fig. 1d) pairing a candidate
82 molecular catalyst that can bind N_2 (M−N_2) and facilitate its multistep reduction to NH_3 through
83 various M−N_xH_y intermediates (e.g., M−N=NH, M=NNH_2, M=NH),[9] with a CPET mediator that
84 interfaces the electrode and the acid with the N_2 reduction cycle via critical CPET steps.
85 Importantly, certain N_2RR intermediates are challenging to move through the cycle; they can be
86 difficult to independently reduce or protonate (vide infra). In principle, a CPET step can
87 circumvent this issue and favorably shift the overpotential needed to drive the net electrochemical
88 N_2RR process. Here we show the feasibility of this tandem catalysis strategy, demonstrating N_2RR
89 electrocatalysis in solution at room temperature and atmospheric N_2 pressure at a comparatively
90 mild potential (−1.2 V) in the presence of tosic acid.

91 As a model system to test our tandem approach, we adapted the classical tungsten system
92 studied by Pickett.[22] Using **W**$(N_2)_2$ and the same solvent (tetrahydrofuran; THF), electrolyte (0.2
93 M [TBA][BF_4]; TBA = tetra-*N*-butylammonium), and acid (100 equiv TsOH), in the presence of
94 the cobalt CPET mediator, **Co**(III,N)$^+$, a controlled potential electrolysis (CPE) produced 4.7 ± 0.3
95 equiv NH_3 at 18 ± 2% Faradaic efficiency (FE) over a period of 11 hours using a glassy carbon
96 (GC) electrode at −1.35 V (see Supplementary Information, section S4). Reloading the system
97 with an additional 100 equiv TsOH furnished a total of 7.6 equiv NH_3. While further improvements
98 in yield and turnover are discussed next, this initial result shows that inclusion of the **Co**(III,N)$^+$

mediator turns on electrocatalysis by **W**$(N_2)_2$, and at a potential that is 1.25 V positive of Pickett's original work (Fig. 1c). In the absence of the mediator, electrocatalysis is not observed.

To further improve electrocatalytic N_2RR by this tandem **W**$(N_2)_2$/**Co**$(III,N)^+$ co-catalyst system, we canvassed factors including the working electrode, the loading of TsOH, the electrolyte, and the solvent (see Supplementary Information, section S5). We found that boron-doped diamond (BDD) as a working electrode, known to better mitigate background HER than GC,[28] enhanced NH_3 selectivity. Using lithium triflimide ([Li][NTf_2]), which features a hard Lewis acid and a robust, non-coordinating anion, proved favorable to [TBA][BF_4] as the electrolyte. Also, we found dimethoxyethane (DME) to be a more robust ethereal solvent than THF for this electrocatalysis. Optimized conditions (BDD, 0.1 M [Li][NTf_2], DME, 5 mM TsOH, 0.05 mM **W**$(N_2)_2$/**Co**$(III,N)^+$) significantly improved the N_2RR electrocatalysis with 11.5 equiv NH_3 per **W**$(N_2)_2$/**Co** (45% FE) being generated at −1.35 V over 5.5 hours (Fig. 2a,b).

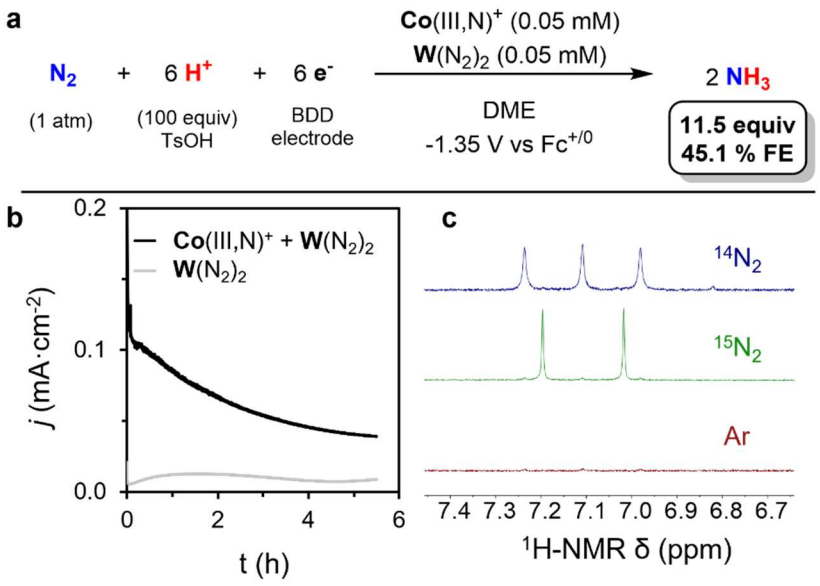

112

113 **Fig. 2. Electrocatalytic N_2RR via tandem catalysis. a**, Electrocatalytic N_2RR upon controlled
114 potential electrolysis (CPE) at −1.35 V vs $Fc^{+/0}$ in 0.1 M [Li][NTf_2] DME solution containing 0.05
115 mM **Co**(III,N)$^+$, 0.05 mM **W**$(N_2)_2$, and 5 mM TsOH, using a BDD plate working electrode. **b**,
116 Current profile for the CPE experiment described (black trace) and a similar CPE experiment in
117 the absence of the **Co**(III,N)$^+$ mediator. **c**, Quantification of NH_3 following CPE via ^{1}H-NMR
118 spectroscopy under previous conditions using either $^{14}N_2$, $^{15}N_2$, or an argon atmosphere.

119 When **Co**(III,N)$^+$ was omitted, only 0.8 equiv NH_3 per **W**$(N_2)_2$ were obtained under these
120 same conditions. Excluding **W**$(N_2)_2$ instead afforded < 0.1 equiv NH_3 per **Co**(III,N)$^+$ (Table S1).
121 Control experiments to assess the purity of the N_2 gas, studying the electrocatalysis under argon
122 instead of N_2 (< 0.1 equiv NH_3 per **W**$(N_2)_2$/**Co**(III,N)$^+$), or under $^{15}N_2$ (8.1 equiv $^{15}NH_3$ per
123 **W**$(N_2)_2$/**Co**(III,N)$^+$), unequivocally demonstrate N_2 as the sole N-source of the NH_3 produced (see
124 Fig. 2c and section S6 of the Supplementary Information). Finally, rinsing the electrodes following
125 a CPE and performing an analogous experiment with fresh acid but in the absence of
126 **W**$(N_2)_2$/**Co**(III,N)$^+$ resulted in no NH_3 production (< 1 nmol). A higher turnover number per

W$(N_2)_2$/**Co**$(III,N)^+$ (up to 39.5) was demonstrated by using a higher surface area GC foam electrode and lowering the catalyst concentration (Table S1).

To assess the electrochemical behavior of the **W**$(N_2)_2$/**Co**$(III,N)^+$ co-catalyst system, a series of cyclic voltammograms (CVs) were performed. Following prior studies, dissolution of **W**$(N_2)_2$ in THF with added TsOH acid quantitatively produces the doubly protonated hydrazido complex (TsO)**W**$(NNH_2)^+$.[23] CVs of (TsO)**W**$(NNH_2)^+$ in a 0.1 M [Li][NTf_2] THF solution on a BDD working electrode show two irreversible one-electron waves at low potential (< −2 V, Fig. 3a). In accord with prior literature, these are presumed due to the generation of **W**$(NNH_2)^+$ and **W**(NNH_2), respectively,[22] where the strongly reducing potential reflects the challenge in reducing the 18-electron, closed-shell (TsO)**W**$(NNH_2)^+$ complex. While the addition of excess TsOH (100 equiv) to the solution containing (TsO)**W**$(NNH_2)^+$ led to an increase in current (irreversible) with an onset at −1.3 V, the same response is observed without added **W** and is due to background HER at the electrode (Fig. 3a). The independent CV of **Co**$(III,N)^+$ in THF shows a reversible $Co^{III/II}$ couple at −1.35 V (Fig. 3b), assigned to **Co**$(III,N)^+$/**Co**(II,N).[26] This couple shifts to −1.21 V when the mediator is protonated at the tethered dimethylaniline group (i.e., **Co**$(III,NH)^{2+}$/**Co**$(II,NH)^+$) (Fig. 3a). Gratifyingly, CVs of (TsO)**W**$(NNH_2)^+$ in the presence of **Co**$(III,N)^+$ result in a fully irreversible, multi-electron wave at −1.2 V (Fig. 3a), consistent with electrocatalytic N_2RR. Interestingly, the reversible CV response of the **Co**$(III,NH)^{2+}$/**Co**$(II,NH)^+$ couple at −1.21 V (in the absence of TsOH) is noticeably altered as (TsO)**W**$(NNH_2)^+$ is added, if scanning at a slow rate (e.g., 5-25 $mV \cdot s^{-1}$); the presence of the **Co**$(III,N)^+$/**Co**(II,N) couple becomes clearly evident (Fig. 3b). The implication is that as **Co**$(II,NH)^+$ is generated in the presence of (TsO)**W**$(NNH_2)^+$ a CPET step occurs that generates **Co**$(III,N)^+$, the CV response of which becomes apparent at scan rates well matched to the kinetics of this chemical step in the absence of acid.

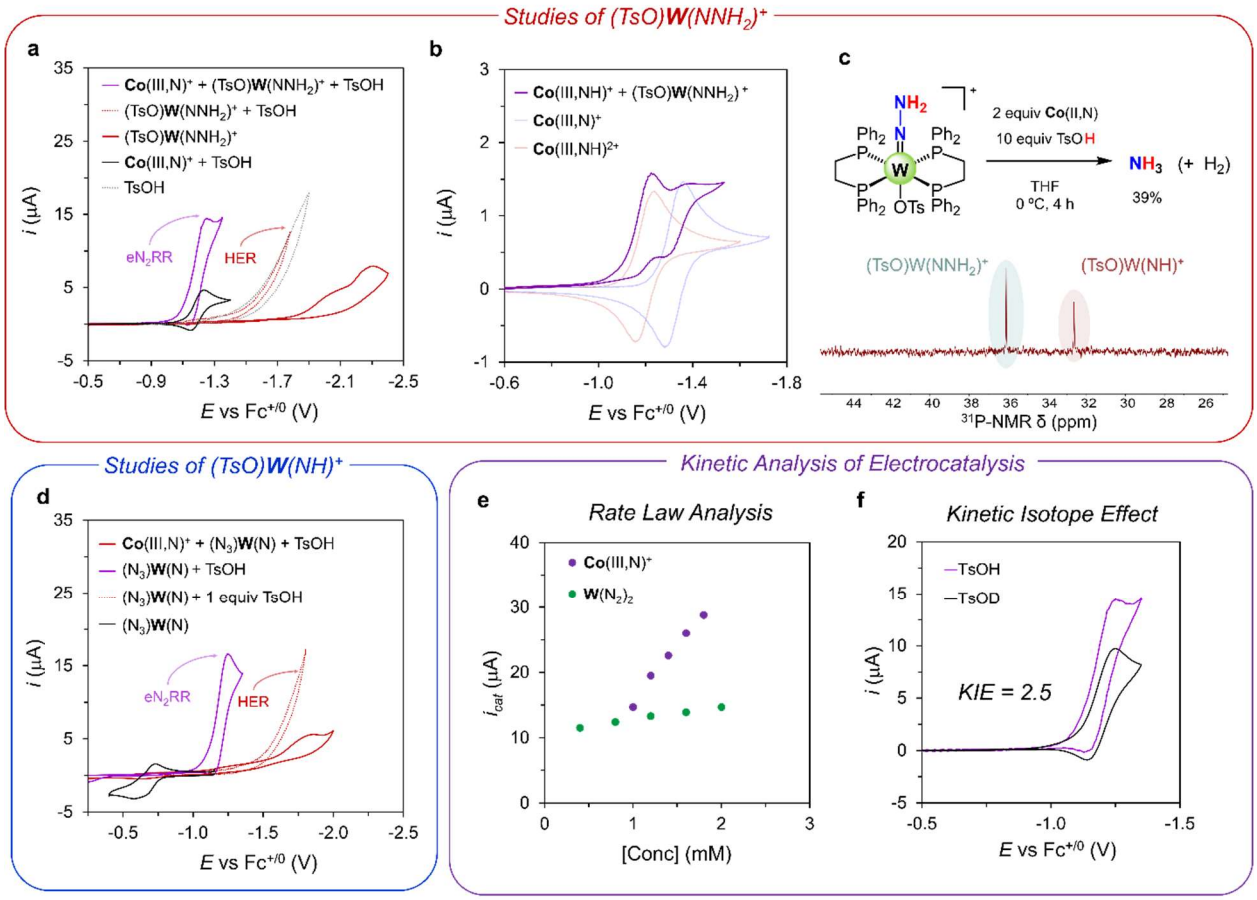

Fig. 3. Mechanistic insights into tandem CPET-N_2RR. a, CV of 50 mM TsOH (dashed grey); 0.5 mM **Co**(III,N)$^+$ with 50 mM TsOH (black); 0.5 mM (TsO)**W**$(NNH_2)^+$ (solid red); 50 mM TsOH and 0.5 mM (TsO)**W**$(NNH_2)^+$ (dashed red); 0.5 mM **Co**(III,N)$^+$/(TsO)**W**$(NNH_2)^+$ and 50 mM TsOH (purple). **b**, CV at 5mV·s^{-1} of 0.5 mM **Co**(II,NH)$^+$/(TsO)**W**$(NNH_2)^+$ (purple trace) compared to 0.5 mM **Co**(II,NH)$^+$ (blue trace) and 0.5 mM **Co**(III,N)$^+$ (red trace). **c**, Chemical reaction of 0.5 mM (TsO)**W**$(NNH_2)^+$ in THF with 2 equiv **Co**(III,N)$^+$ in THF in the presence of excess acid and the corresponding ^{31}P-NMR spectrum. **d**, CV of 0.5 mM (N_3)**W**(N) (black); 0.5 mM (N_3)**W**(N) and 1 equiv TsOH (solid red); 0.5 mM (N_3)**W**(N) and 50 mM TsOH (dashed red); 0.5 mM **Co**(III,N)$^+$/(N_3)**W**(N) and 50 mM TsOH (purple). **e**, Plot of the catalytic current i_{cat} versus the concentration of the different co-catalysts. **f**, CV of 0.5 mM **Co**(III,N)$^+$/(TsO)**W**$(NNH_2)^+$ with

either 50 mM TsOH (purple) or TsOD (black). **Note:** All CVs in A-F were performed at 100 $mV \cdot s^{-1}$ (unless otherwise stated) in 0.1 M [Li][NTf_2] THF solution using a BDD disk as the working electrode, Pt disk as the counter electrode and Ag/AgOTf (5mM) as the reference electrode.

To independently probe this issue, we generated (TsO)**W**$(NNH_2)^+$ in THF with excess TsOH present, and added two equiv of **Co**(II,N) to the solution, conditions under which **Co**$(II,NH)^+$ is instantly generated. Such a reaction liberates 0.39 equiv NH_3 per (TsO)**W**$(NNH_2)^+$ (Fig. 3c) over 4 hrs (note: this experiment was performed at 0 °C to attenuate competing HER). Analysis of the reaction mixture by ^{31}P-NMR spectroscopy showed some remaining (TsO)**W**$(NNH_2)^+$ starting material and also a new peak corresponding to the imido complex (TsO)**W**$(NH)^+$. The identity of the latter species was confirmed by its independent generation via the protonation of the nitride precursor (N_3)**W**(N) with TsOH (Fig. S47).[29] While other processes are presumably operative in this reaction (e.g., HER and CPET or proton-transfer (PT) steps to other W−N_xH_y intermediates), the experiment correlates well with the CV response noted above, suggesting CPET to (TsO)**W**$(NNH_2)^+$ occurs, presumably followed by N−N cleavage and NH_3 release (Eq. 1 below depicts one plausible scenario). Such a CPET step helps explain why the system can be turned over at −1.2 V, whereas one-electron reduction of (TsO)**W**$(NNH_2)^+$ requires a potential of −2 V.

$$\mathbf{W}{=}\mathrm{N}{-}\mathrm{NH_2}^+ + \mathbf{Co}(\mathrm{II,NH})^+ \longrightarrow \mathbf{W}{\equiv}\mathrm{N}^+ + \mathrm{NH_3} + \mathbf{Co}(\mathrm{III,N})^+ \qquad (1)$$

Relatedly, the CV of the previously reported nitride complex (N_3)**W**(N) shows a reversible redox wave at −0.8 V that shifts to −1.8 V upon addition of 1 equiv of TsOH to generate (X)**W**$(NH)^+$ (X = N_3^- or OTs^-; Fig. 3d).[29–31] Including 1 equiv of **Co**$(III,N)^+$ and excess TsOH with in situ generated (TsO)**W**$(NH)^+$ yields the same multielectron electrocatalytic wave at −1.2 V

observed with (TsO)**W**(NNH_2)$^+$. Additionally, the reaction of (N_3)**W**(N) with 4 equiv of **Co**(II,N) in the presence of excess TsOH afforded 0.79 equiv NH_3 per **W**, along with (TsO)**W**(NNH_2)$^+$ and (TsO)**W**(NH)$^+$ detected via ^{31}P-NMR spectroscopy (Fig. S49). These experiments establish that an imide intermediate of the type (TsO)**W**(NH)$^+$ can cycle through the downstream half of the N_2RR cycle at −1.2 V to regenerate **W**(N_2)$_2$, which is then protonated to form (TsO)**W**(NNH_2)$^+$ by the excess acid. CPET from **Co**(II,NH)$^+$ to (TsO)**W**(NH)$^+$ likely initiates this process given the 1-electron reduction potential (~ −1.8 V) for an (X)**W**(NH)$^+$ species is presumably inaccessible at our operating potential.

Kinetic analysis of N_2RR electrocatalysis observed is difficult due to the $6H^+/6e^-$ nature of the process, obscuring analytical solutions to the relationship between the catalytic current (i_{cat}) and the kinetic rate (k_{obs}); such an analysis is further obfuscated by the use of two co-(electro)catalysts working in tandem (see Supplementary Information, section S2). Nonetheless, by independently varying the concentration of the **W**(N_2)$_2$ and **Co**(III,N)$^+$, we could determine a positive order for both co-catalysts in the electrocatalytic response (Fig. 3e). Interestingly, a positive order in acid was also evident (Fig. S60), as was a primary kinetic isotope effect (2.5) when comparing TsOH vs TsOD (Fig. 3f). These electrochemical and chemical data presented in total are consistent with one or perhaps two rate-contributing CPET steps, involving (TsO)**W**(NNH_2)$^+$ and possibly also (TsO)**W**(NH)$^+$, and a rate-contributing protonation step (such as initial protonation of **W**(N_2)$_2$; see Supplementary Information, section S7).

To explore this tandem *e*CPET-N_2RR strategy more broadly, we turned our attention to a series of complexes known to mediate catalytic N_2RR in the presence of various reductant/acid reagents (Fig. 4a). We opted to test them under the standard conditions (Fig. 2a; using 0.05 mM of the N_2RR co-catalyst in place of **W**(N_2)$_2$), reasoning that some degree of electrocatalysis might

turn on at −1.2 V if CPET steps from **Co**(II,NH)$^+$ can circumvent the need for challenging ET steps requiring more negative potentials.

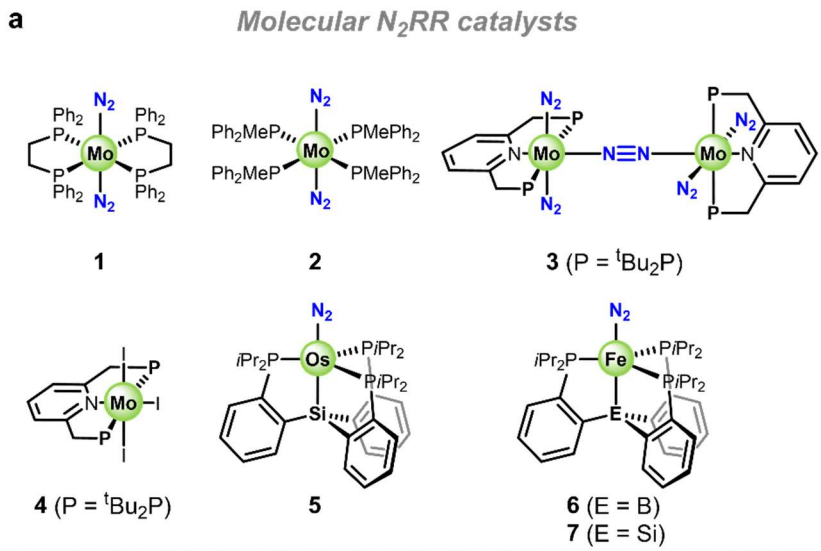

b

N_2 + HOTs → NH_3

(1 atm) (100 equiv)

[Co] (0.05 mM)
[Cat] (0.05 mM)
DME
BDD(-)/Zn(+)
-1.35 V vs $Fc^{+/0}$

Catalyst	equiv NH_3/Cat	FE (%)
W$(N_2)_2$	11.5	45.1
W$(N_2)_2^*$	39.5	42.9
1	12.9	50.5
2	14.0	54.8
3	8.7	34.0
4	<0.1	<1.0
5	5.6	21.9
6	4.5	17.6
7	1.5	4.5

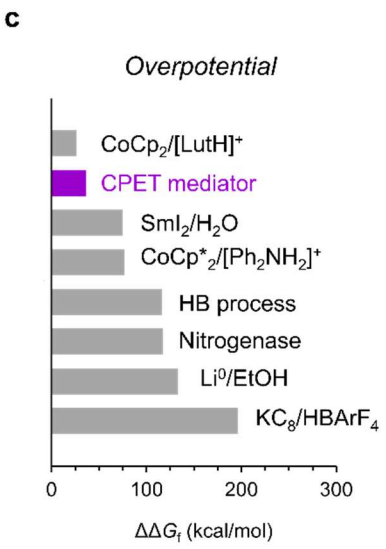

Fig. 4. Electrocatalytic N_2RR using reported molecular catalysts. a, Molecular N_2RR catalysts explored in combination with the cobalt CPET mediator under electrocatalytic conditions. **b,** Results of the electrocatalytic experiments for each molecular catalyst upon controlled potential electrolysis at −1.35 V vs $Fc^{+/0}$ in 0.1 M [Li][NTf_2] DME solution containing 0.05 mM **Co**(III,N)$^+$, 0.05 mM of N_2RR catalyst, and 5 mM TsOH, using a BDD plate working electrode. *A GC foam

was used as the working electrode instead and the concentration was 0.01 mM for both co-catalysts and 1 mM TsOH. **c**, Estimated overpotential ($\Delta\Delta G_f$) for N_2RR including the tandem *e*CPET strategy reported here, the HB process (which includes H_2 generation), a nitrogenase enzyme, Li-mediated N_2RR using EtOH as the H^+ source, and various reductant and acid partners used in chemically driven N_2RR.

To probe this, we examined the group VIII complexes **Fe**(N_2) and **Os**(N_2), where **Fe** and **Os** feature tris(phosphine)borane and silane ligands, respectively (Fig. 4a). Each mediates N_2RR at −78 °C but requires a comparatively strong reductant (Cp^*_2Co at −2 V) owing to an M−$N_2^{0/-}$ couple that is key to moving through their respective N_2RR cycles via an electron transfer-proton transfer pathway (Eq. 2 and 3).[32,33] Such a pathway is not feasible at −1.2 V. Strikingly, both **Fe** and **Os** display an electrocatalytic wave at −1.2 V (see Supplementary Information, section S10), akin to **W**(N_2)$_2$, and CPE at −1.35 V produced 5.6 and 4.5 equiv NH_3, respectively (Fig. 4b). Despite their relatively lower selectivity for NH_3 generation compared to **W**(N_2)$_2$, for which these conditions were optimized, the electrocatalysis observed represents a remarkable shift in thermodynamic efficiency for the overall N_2RR cycle relative to previously reported conditions using Cp^*_2Co and $Ph_2NH_2^+$ (vide infra). To explain this, we posit that the neutral M−N_2 adduct species are converted directly to M−N=NH intermediates via CPET from **Co**(II,NH)$^+$, circumventing the M−$N_2^{0/-}$ couple in the cycle (Eq. 4).[32] As a counter example, a related tris(phosphine)silyl iron-N_2 complex, (SiP_3)Fe−N_2, is electrocatalytically inactive under standard conditions, presumably due to the generation of an undesired (SiP_3)Fe(H)(N_2) state which cannot be moved through the N_2RR cycle.[12,34]

$$\mathbf{M}\text{—}N_2 + e^- \xrightarrow{< -2V} \mathbf{M}\text{—}N_2^- \qquad (2)$$

$$\mathbf{M}\text{—}N_2 + H^+ \longrightarrow \mathbf{M}\text{—}N_2H \qquad (3)$$

$$\mathbf{M}\text{—}N_2 + \mathbf{Co}(II,NH)^+ \longrightarrow \mathbf{M}\text{—}N_2H + \mathbf{Co}(III,N)^+ \qquad (4)$$

For **Fe** specifically, generation of the on-path **Fe**−N_2 species requires reduction of the $\mathbf{Fe}^+$ pre-catalyst used here, which occurs at ca. −1.4 V (see Supplementary Information, section S10). Thus, applying slightly more bias in the CPE (−1.45 V instead of −1.35 V) results in improved NH_3 yield (9.3 equiv NH_3 per **Fe**). The results for **Fe** described in this study are distinct from our previous study.[17] When exploring the addition of Cp^*_2Co to **Fe** as a potential PCET mediator, a slightly enhanced yield was observed relative to when Cp^*_2Co was not added, but a potential of −2.1 V remained necessary, indicating that accessing the Fe−N_2^- anion was still required.

We also explored a series of Mo complexes, including two tetrakis(phosphine) systems that are structurally related to **W**$(N_2)_2$ (compounds **1** and **2** in Fig. 4a), and highly active pincer-type bis(phosphine)pyridine complexes pioneered more recently.[11,35] Among the reductants that have proven effective for these systems, SmI_2/H_2O has led to the most impressive results in chemically (as opposed to electrochemically) driven catalysis.[36,37] We find that the **Mo**$(N_2)_2$ complexes (**1**) and (**2**) are both effective co-electrocatalysts with impressive selectivities, furnishing 12.9 and 14.0 equiv NH_3 (50.5 and 54.8% FE for NH_3), respectively. A dinuclear Mo catalyst system (**3**) also displays electrocatalysis under these conditions (8.7 equiv NH_3 per Mo).[11] By contrast, the mononuclear triiodide complex (**4**), which has been demonstrated to be highly active for N_2RR,[36] is electrocatalytically inactive under these conditions (< 0.1 equiv NH_3 detected). The latter observation is readily explained; the strong reduction potential (−1.8 V) required to access an on-path N_2RR intermediate by iodide loss is not accessible at −1.35 V.[38]

The free energy for the electrocatalytic N_2RR processes described here compares quite favorably to estimates for other systems that mediate catalytic and electrocatalytic N_2RR. This can be readily quantified by $\Delta\Delta G_F(NH_3)$, a term that compares the energetic input for N_2RR relative to a reaction that derives the needed protons and electrons from H_2 (Eq. 5).[39,40] Using the bond dissociation free energy (BDFE) for H_2 (102.5 kcal/mol) [41] and that of the CPET mediator **Co**(II,NH)$^+$ (38.9 kcal/mol), [26] the $\Delta\Delta G_F(NH_3)$ is 36.5 kcal/mol for the electrocatalysis observed at −1.2 V by our CV studies. This net driving force is at least 50 kcal/mol lower than has been reported for most other reductant/acid cocktails used with synthetic N_2RR catalyst systems (Fig. 4c): SmI_2/H_2O (75 kcal/mol), $Cp^*_2Co/[Ph_2NH_2]^+$ (77 kcal/mol), $KC_8/HBAr^F_4$ (196 kcal/mol) (BAr^F_4 = $B(3,5\text{-}(CF_3)_2\text{-}C_6H_3)_4$).[32,42] A crude comparison with the biological nitrogenases (~117 kcal/mol accounting for ATP) and the industrial HB process (~116 kcal/mol when considering *both* H_2 production and N_2 reduction) is also favorable.[43] Likewise, heterogeneous systems based on Li^+/Li ($E°(Li^{+/0})$ < −3.7 V), which commonly utilize with ethanol as the acid, operate at an estimated $\Delta\Delta G_F(NH_3)$ = 133 kcal/mol.[7,44] Interestingly, one combination of reductant and acid, Cp_2Co and lutidinium, first studied in the Schrock system and later applied towards N_2RR catalysis with the Nishibayashi bis(phosphine)pyridine molybdenum catalyst studied herein (complex **3** in Fig. 4),[10,11] is thermally favorable by comparison ($\Delta\Delta G_F(NH_3)$ = 26 kcal/mol). This suggests that alternative acids and mediator designs may yet improve the efficiency achievable by tandem electrocatalysis.

$$\Delta\Delta G_f(NH_3) = 3 \cdot [BDFE(H_2)/2 - BDFE_{eff}] \quad (5)$$

It is widely appreciated that CPET steps can offer thermodynamic advantages relative to distinct ET-PT or PT-ET pathways in enzyme catalysis, where multielectron redox reactions must be driven at biologically accessible potentials,[45] and also in synthetic catalyst systems.[9] The

tandem catalytic approach to N_2RR via *e*CPET described herein provides a vivid example of the latter, where an *e*CPET step turns on catalysis that is otherwise inaccessible at the applied potential. A comparison with nitrogenase enzymes is illustrative here. It has been posited that the active-site cofactors of nitrogenases store-up proton and electron equivalents via H-atoms bound at or near to the active-site cluster to be able to mediate N_2 reduction at a single redox potential (set by the potential of the Fe-protein).[46] Our two-component tandem catalyst system functions in a conceptually similar manner, where the mediator independently stores an H-atom equivalent at a given potential for delivery to a synthetic M−N_2 "active site". While we expect this approach to small molecule reductive catalysis via *e*CPET may prove more general, exciting opportunities remain for fundamental progress and practical applications. For instance, the rate of the N_2RR electrocatalysis described here at −1.2 V, while remarkable compared to background, should be possible to enhance. In this context, fundamental studies towards developing new tandem co-catalysts, and studies aimed at improving the electrolyte, acid, and electrode interface, should prove fruitful.

Methods

General methods. All manipulations were carried out using standard Schlenk or glovebox techniques under an N_2 or Ar atmosphere as specified. Solvents were deoxygenated and dried by thoroughly sparging with N_2 followed by passage through an activated alumina column in a solvent purification system by SG Water, USA LLC. Subsequently, the solvents were further dried and stored under N_2 atmosphere inside a glove box with molecular sieves obtained from Sigma Aldrich that were activated at 200ºC overnight under vacuum. Non-halogenated solvents were tested with sodium benzophenone ketyl in tetrahydrofuran (THF) in order to confirm the absence of oxygen and water. Deuterated d_6-DMSO solvent (D, 99.9% with a purity of 99.5%) was purchased from

Cambridge Isotope Laboratories, Inc., and use as received. Isotope labelled $^{15}N_2$ gas cylinder was purchased from Cambridge Isotope Laboratories, Inc., NLM-363-1-LB, PSO #:21A-0223, Lot #: I-24583/A R0664758.

N_2 gas in a NEXUS glovebox (Vacuum Atmospheres Company) was purified by a Nexus modular purification system. The purity of N_2 gas was assessed via colorimetric, gas chromatography and NMR methods, with regard to NH_3, N_2O, NO_2^- and NO_3^- impurities.

Cobaltocenium hexafluorophosphate ($[Cp_2Co][PF_6]$), triflic acid, ferrocene, silver triflate, tetrabutylammonium tetrafluoroborate ($[TBA][BF_4]$; TBA = tetra-*N*-butylammonium), lithium perchlorate ($[Li][ClO_4]$), tosic acid (TsOH) were all used as purchased from Sigma Aldrich. [Li][OTf] (OTf = trifluoromethanesulfonate) and $[Li][NTf_2]$ (NTf_2 = bis(trifluoromethanesulfonyl)imide) were also obtained from Sigma Aldrich and further dried under vacuum at 100 ºC for 120 h prior use. Tetrabutylammonium hexafluorophosphate ($[TBA][PF_6]$) from Sigma Aldrich was recrystallized from ethanol prior to use. Silver triflate (AgOTf) was purchased from Strem and used without further purification. The absence of any detectable NH_4^+, NO_3^- or NO_2^- impurities in the electrolyte solution coming from either solvent, electrolyte or acid was analyzed by subjecting the solutions to NH_4^+ detection via ^{1}H-NMR spectroscopy and NO_2^-/NO_3^- detection via the Griess method (*vide infra*). Whenever water was specified as solvent, deionized water OmniSolv (Supelco, Sigma Aldich) was used to prepare the solutions.

<u>* Cited literature for the preparation of known inorganic compounds:</u>

$(Cp)Co(Cp^N)$,[26] $[(Cp)Co(Cp^N)][OTf]$,[26] $[(Cp)Co(Cp^{NH})][OTf]_2$,[26] $[(dppe)_2W(N_2)_2]$,[23] $[(dppe)_2W(NNH_2)(OTs)]$,[47] $[(dppe)_2W(N)(N_3)]$,[29] $[(dppe)_2Mo(N_2)_2]$,[23] $[(PPh_2Me)_4Mo(N_2)_2]$,[48] $[Mo(N_2)_2(PNP)]_2(\mu\text{-}N_2)$,[11] $[Mo(I)_3(PNP)]$,[36] $(P_3Si)Os(N_2)$,[49] $[(P_3B)Fe]^+$,[12] $(P_3Si)Fe(N_2)$,[50]

[Na][BAr^F_4] (BAr^F_4 = B(3,5-$(CF_3)_2$-$C_6H_3)_4$),[51] and TsOD[52] were synthesized as described previously.

Reagents for the Griess method for NO_2^- quantification were purchased from Sigma Aldrich and include: sulphanilamide, HCl solution (32 wt.%), and N-1-naphthylenthylenediamine dihydrochloride. Two solutions where prepared for the colorimetric method according to the literature procedure[53]: the first one containing 0.1 g of sulphanilamide in 1 mL HCl solution, adjusting the final volume to 10 mL with deionized water; the second contains 10 mg of N-1-naphthylenthylenediamine dihydrochloride in 10 mL of deionized water. Both solutions were stored in amber bottle and refrigerated. For NO_3^- quantification, a solution containing 0.02 wt.% VCl_3 in 6 M HCl was also employed to quantitatively reduce NO_3^- to NO_2^-.

^{1}H-NMR spectra were recorded with a Varian 400 MHz spectrometer and chemical shifts are reported in ppm relative to tetramethylsilane, using ^{1}H resonances from residual solvent as internal standards. ^{31}P NMR spectra were also recorded with Varian 400 MHz and referenced to the H_3PO_4 signal. For detection of NH_4^+, 1,3,5-trimethoxybenzene was employed as an internal standard, purchased from Sigma Aldrich and used as received; a solution of 8 M H_2SO_4 (98%, Thermo Fischer Scientific) in d_6-DMSO was employed to control the final pH of the NMR sample.[54]

Measurements were taken on a Cary 50 UV-visible spectrophotometer using a 1 cm quartz cell sealed with a Teflon stopcock.

Gas chromatography coupled to a thermal conductivity detector (GC-TCD) was employed to detect for possible contamination of N_2O in the $^{14}N_2$ and $^{15}N_2$ gas supply. A 100 μL Hamilton syringe was used to sample the headspace and to inject into the GC-TCD. GC-TCD was performed

in the Environmental Analysis Center (Caltech) using a HP 5890 Series II instrument with Helium as the carrier gas. Calibration was determined by direct injection of known volumes of N_2O.

Electrochemistry. A CHI instruments 600B and a Biologic VSP potentiostat were used for all electrochemical data collection.

Cyclic voltammetry (CV) experiments were carried out in a one-compartment three-electrode cell using a boron doped diamond (BDD) disk as the working electrode (3 mm diameter), a Pt disk as the counter electrode, and a Ag/AgOTf (5 mM) reference electrode. Details for the CVs are noted as they appear. For all measurements IR compensation was applied accounting for 85% of the total resistance. All the reported potentials are referenced to the ferrocenium/ferrocene couple ($Fc^{+/0}$) used as an external standard.

Controlled potential coulometries (CPCs) were carried out in a gas-tight, two-compartment or H-cell equipped with a frit to separate anodic from cathodic chambers (Fig. S1). This cell also features two necks, one in each compartment, sealed using a septum that allows for bubbling of different gasses other than the $^{14}N_2$, such as Argon and $^{15}N_2$, needed in control experiments. Either a BDD plate (dimensions 1x1 cm) or a high surface area reticulated vitreous carbon foam was employed as the working electrode, a Ag/AgOTf (5 mM) as the reference electrode, and a Zn plate as the sacrificial counter electrode. In a typical experiment, 6 mL of solvent containing 0.2-0.1 M of the specified electrolyte and the tosic acid was added to the electrochemical cell, 3 mL per compartment. For experiments including the catalysts, the cathodic chamber was also charged with the corresponding amount of **Co**(III,N)$^+$ mediator and **W**$(N_2)_2$ (or other N_2RR catalyst), or both were taken from concentrated stock solutions (1 mg/mL). The electrochemical cell was assembled inside an N_2 glove box in which the CPC experiment was also performed. The potential applied

during the CPC experiment was set to −1.35 V vs $Fc^{+/0}$ according to the peak current observed for the catalytic wave from previous CVs. The solution was stirred throughout the CPC experiment.

The BDD disk electrode for cyclic voltammetry was polished using a PK-3 polishing kit with 6 μm diamond (Biologic). The BDD plate electrodes were pre-treated according to literature procedures.[55] The Zn counter electrode was polished with a stainless steel sponge, washed repeatedly with water and acetone and vacuum dried.

Ammonia quantification. Upon completion of CPC experiments, excess of acid (twice as much as the theoretical amount of ammonia produced) was added through the septum with a syringe in order to quench all possible free ammonia in solution as NH_4^+. Subsequently, the cell was place in a cold well at −78 ºC using a dry ice/acetone bath in order to condense possible evaporated ammonia in the headspace. After 10 min at this temperature, the electrochemical cell was brought to room temperature and allowed to stir for another 10 min in the presence of the excess acid. The solution was then transferred with a pipette into a Schlenk tube; the cell was subsequently washed with more solvent that was also collected into the same tube. The tube was tightly sealed with a Kontes cap, brought out of the glove box and placed into liquid N_2 allowing 10 min for the entire solution to freeze. Once frozen, the Schlenk tube was opened and 2 equivalents of sodium *tert*-butoxide (NaO^tBu_4) base per mol of total acid (initial acid loading plus quenching acid) were slowly delivered in the form a 2.5 M MeOH solution, leaving 5 min at liquid nitrogen temperature for equilibration. Afterwards, the headspace of the tube was evacuated to constant pressure and the tube was closed and brought to room temperature, stirring for 10 min to react all the NH_4^+ with the added base to liberate NH_3. At the same time, in a different tube, 2 mL of a 2.0 M HCl solution in diethyl ether was prepared. In the next step the NH_3 solution was vacuum transferred to the ethereal HCl solution to remove non-volatile components of the reaction

mixture, including the catalysts, the electrolyte, the resulting sodium tosylate (NaOTs) and the excess of NaO^tBu_4. The resultant solution (NH_3 and ethereal HCl) was allowed to react for 10 min at room temperature and then evaporated to dryness, affording NH_4Cl. The latter was extracted with 0.5 mL of 1 mM 1,3,4-trimethoxybenzene (TMB) in d_6-DMSO for ^{1}H-NMR analysis. Analysis of the total amount of NH_3 produced after isolation via vacuum transfer overcomes some of the challenges associated with low ammonia concentrations or interferences of the electrolyte solution in the quantification methods when direct sampling from the electrolyte solution is employed for the analysis.[56] Moreover, the amounts of NH_3 produced in the present work are well above those of background levels (Supplementary Information, section S6). Nonetheless, appropriate control experiments have been carried out in order to verify the source of the generated NH_3 as a result of electrocatalytic N_2RR (Supplementary Information, section S6).

Data availability: The datasets generated during and/or analysed during the current study are available from the corresponding author on reasonable request.

References

1. Erisman, J. W., Sutton, M. A., Galloway, J., Klimont, Z. & Winiwarter, W. How a century of ammonia synthesis changed the world. *Nat. Geosci.* **1**, 636–639 (2008).
2. Chen, J. G. *et al.* Beyond fossil fuel–driven nitrogen transformations. *Science* **360**, 873–879 (2018).
3. Service, R. F. Ammonia—a renewable fuel made from sun, air, and water—could power the globe without carbon. *Science | AAAS* https://www.sciencemag.org/news/2018/07/ammonia-renewable-fuel-made-sun-air-and-water-could-power-globe-without-carbon (2018).
4. Martín, A. J., Shinagawa, T. & Pérez-Ramírez, J. Electrocatalytic reduction of nitrogen: from Haber-Bosch to ammonia artificial leaf. *Chem* **5**, 263–283 (2019).

5. Qing, G. *et al.* Recent advances and challenges of electrocatalytic N_2 reduction to ammonia. *Chem. Rev.* **120**, 5437–5516 (2020).
6. Deng, J., Iñiguez, J. A. & Liu, C. Electrocatalytic nitrogen reduction at low temperature. *Joule* **2**, 846–856 (2018).
7. Lazouski, N., Schiffer, Z. J., Williams, K. & Manthiram, K. Understanding continuous lithium-mediated electrochemical nitrogen reduction. *Joule* **3**, 1127–1139 (2019).
8. Ren, Y. *et al.* Strategies to suppress hydrogen evolution for highly selective electrocatalytic nitrogen reduction: challenges and perspectives. *Energy Environ. Sci.* **14**, 1176–1193 (2021).
9. Chalkley, M. J., Drover, M. W. & Peters, J. C. Catalytic N_2-to-NH_3 (or -N_2H_4) Conversion by well-defined molecular coordination complexes. *Chem. Rev.* **120**, 5582–5636 (2020).
10. Yandulov, D. V. & Schrock, R. R. Catalytic reduction of dinitrogen to ammonia at a single molybdenum center. *Science* **301**, 76–78 (2003).
11. Arashiba, K., Miyake, Y. & Nishibayashi, Y. A molybdenum complex bearing PNP-type pincer ligands leads to the catalytic reduction of dinitrogen into ammonia. *Nat. Chem.* **3**, 120–125 (2010).
12. Anderson, J. S., Rittle, J. & Peters, J. C. Catalytic conversion of nitrogen to ammonia by an iron model complex. *Nature* **501**, 84–7 (2013).
13. Lee, Y. S. *et al.* Electroenzymatic nitrogen fixation using a MoFe protein system immobilized in an organic redox polymer. *Angew. Chem. Int. Ed.* **59**, 16511–16516 (2020).
14. Lindley, B. M. *et al.* Mechanism of chemical and electrochemical N_2 splitting by a rhenium pincer complex. *J. Am. Chem. Soc.* **140**, 7922–7935 (2018).
15. Merakeb, L. & Robert, M. Advances in molecular electrochemical activation of dinitrogen. *Curr. Opin. Electrochem.* **29**, 100834 (2021).
16. Bruch, Q. J. *et al.* Considering electrocatalytic ammonia synthesis via bimetallic dinitrogen cleavage. *ACS Catal.* **10**, 10826–10846 (2020).

17. Chalkley, M. J., Del Castillo, T. J., Matson, B. D. & Peters, J. C. Fe-mediated nitrogen fixation with a metallocene mediator: exploring pKa effects and demonstrating electrocatalysis. *J. Am. Chem. Soc.* **140**, 6122–6129 (2018).
18. Helm, M. L., Stewart, M. P., Bullock, R. M., DuBois, M. R. & DuBois, D. L. A synthetic nickel electrocatalyst with a turnover frequency above 100,000 s^{-1} for H_2 production. *Science* **333**, 863–866 (2011).
19. Francke, R., Schille, B. & Roemelt, M. Homogeneously catalyzed electroreduction of carbon dioxide—methods, mechanisms, and catalysts. *Chem. Rev.* **118**, 4631–4701 (2018).
20. Pegis, M. L., Wise, C. F., Martin, D. J. & Mayer, J. M. Oxygen reduction by homogeneous molecular catalysts and electrocatalysts. *Chem. Rev.* **118**, 2340–2391 (2018).
21. Benson, E. E., Kubiak, C. P., Sathrum, A. J. & Smieja, J. M. Electrocatalytic and homogeneous approaches to conversion of CO_2 to liquid fuels. *Chem. Soc. Rev.* **38**, 89–99 (2008).
22. Pickett, C. J. & Talarmin, J. Electrosynthesis of ammonia. *Nature* **317**, 652–653 (1985).
23. Becker, J. Y. & Avraham (Tsarfaty), S. Nitrogen fixation: Part III. Electrochemical reduction of hydrazido (-NNH_2) Mo and W complexes. Selective formation of NH_3 under mild conditions. *J. Electroanal. Chem. Interf. Electrochem.* **280**, 119–127 (1990).
24. Wang, Y. *et al.* Scaling relationships for binding energies of transition metal complexes. *Catal. Lett.* **146**, 304–308 (2016).
25. Kuriyama, S. *et al.* Catalytic formation of ammonia from molecular dinitrogen by use of dinitrogen-bridged dimolybdenum–dinitrogen complexes bearing PNP-pincer ligands: remarkable effect of substituent at PNP-pincer ligand. *J. Am. Chem. Soc.* **136**, 9719–9731 (2014).
26. Chalkley, M. J., Garrido-Barros, P. & Peters, J. C. A molecular mediator for reductive concerted proton-electron transfers via electrocatalysis. *Science* **369**, 850–854 (2020).

27. Derosa, J., Garrido-Barros, P. & Peters, J. C. Electrocatalytic reduction of C–C π-bonds via a cobaltocene-derived concerted proton–electron transfer mediator: fumarate hydrogenation as a model study. *J. Am. Chem. Soc.* **143**, 9303–9307 (2021).
28. Martin, H. B., Argoitia, A., Landau, U., Anderson, A. B. & Angus, J. C. Hydrogen and oxygen evolution on boron-doped diamond electrodes. *J. Electrochem. Soc.* **143**, L133–L136 (1996).
29. Bevan, P. C., Chatt, J., Dilworth, J. R., Henderson, R. A. & Leigh, G. J. The preparation and reactions of azidobis[1,2-bis(diphenylphosphino)-ethane]nitridotungsten(IV). *J. Chem. Soc., Dalton Trans.* 821–824 (1982).
30. Mohammed, M. Y. & Pickett, C. J. From metal imides and molecular nitrogen to ammonia and dinitrogen complexes. *J. Chem. Soc., Chem. Commun.* 1119–1121 (1988).
31. Alias, Y. *et al.* Electrochemistry of molybdenum imides: cleavage of molybdenum–nitrogen triple bonds to release ammonia or amines. *J. Chem. Soc., Dalton Trans.* 4807–4816 (1997).
32. Chalkley, M. J., Del Castillo, T. J., Matson, B. D., Roddy, J. P. & Peters, J. C. Catalytic N_2-to-NH_3 conversion by Fe at lower driving force: a proposed role for metallocene-mediated PCET. *ACS Cent. Sci.* **3**, 217–223 (2017).
33. Fajardo Jr., J. & Peters, J. C. Catalytic nitrogen-to-ammonia conversion by osmium and ruthenium complexes. *J. Am. Chem. Soc.* **139**, 16105–16108 (2017).
34. Fong, H., Moret, M.-E., Lee, Y. & Peters, J. C. Heterolytic H_2 cleavage and catalytic hydrogenation by an iron metallaboratrane. *Organometallics* **32**, 3053–3062 (2013).
35. Chatt, J. & Leigh, G. J. Nitrogen fixation. *Chem. Soc. Rev.* **1**, 121–144 (1972).
36. Ashida, Y., Arashiba, K., Nakajima, K. & Nishibayashi, Y. Molybdenum-catalysed ammonia production with samarium diiodide and alcohols or water. *Nature* **568**, 536–540 (2019).
37. Ashida, Y. *et al.* Molybdenum-catalyzed ammonia formation using simple monodentate and bidentate phosphines as auxiliary ligands. *Inorg. Chem.* **58**, 8927–8932 (2019).

38. Arashiba, K. *et al.* Catalytic nitrogen fixation via direct cleavage of nitrogen–nitrogen triple bond of molecular dinitrogen under ambient reaction conditions. *Bull. Chem. Soc. Jpn.* **90**, 1111–1118 (2017).
39. Chalkley, M. J. & Peters, J. C. Relating N–H bond strengths to the overpotential for catalytic nitrogen fixation. *Eur. J. Inorg. Chem.* 1353–1357 (2020).
40. Pappas, I. & Chirik, P. J. Catalytic proton coupled electron transfer from metal hydrides to titanocene amides, hydrazides and imides: determination of thermodynamic parameters relevant to nitrogen fixation. *J. Am. Chem. Soc.* **138**, 13379–13389 (2016).
41. Warren, J. J., Tronic, T. A. & Mayer, J. M. Thermochemistry of proton-coupled electron transfer reagents and its implications. *Chem. Rev.* **110**, 6961–7001 (2010).
42. Kolmar, S. S. & Mayer, J. M. $SmI_2(H_2O)_n$ reduction of electron rich enamines by proton-coupled electron transfer. *J. Am. Chem. Soc.* **139**, 10687–10692 (2017).
43. van der Ham, C. J. M., Koper, M. T. M. & Hetterscheid, D. G. H. Challenges in reduction of dinitrogen by proton and electron transfer. *Chem. Soc. Rev.* **43**, 5183–5191 (2014).
44. Lazouski, N., Chung, M., Williams, K., Gala, M. L. & Manthiram, K. Non-aqueous gas diffusion electrodes for rapid ammonia synthesis from nitrogen and water-splitting-derived hydrogen. *Nat. Catal.* **3**, 463–469 (2020).
45. Reece, S. Y. & Nocera, D. G. Proton-coupled electron transfer in biology: results from synergistic studies in natural and model systems. *Annu. Rev. Biochem.* **78**, 673–699 (2009).
46. Lanzilotta, W. N., Christiansen, J., Dean, D. R. & Seefeldt, L. C. Evidence for coupled electron and proton transfer in the [8Fe-7S] cluster of nitrogenase. *Biochemistry* **37**, 11376–11384 (1998).
47. Lane, J. D. & Henderson, R. A. Mechanism of the reaction between trans-$[W(NNH_2)(p\text{-}MeC_6H_4SO_3)(Ph_2PCH_2CH_2PPh_2)_2]^+$ and NEt_3: the influence of the metal on the rates of proton transfer of hydrazido(2–)-ligands. *J. Chem. Soc., Dalton Trans.* 197–200 (1987).

48. Ning, Y., Sarjeant, A. A., Stern, C. L., Peterson, T. H. & Nguyen, S. T. One-pot synthesis of Mo^0 dinitrogen complexes possessing monodentate and multidentate phosphine ligands. *Inorg. Chem.* **51**, 3051–3058 (2012).
49. Takaoka, A., Gerber, L. C. H. & Peters, J. C. Access to well-defined ruthenium(I) and osmium(I) metalloradicals. *Angew. Chem. Int. Ed.* **49**, 4088–4091 (2010).
50. Whited, M. T., Mankad, N. P., Lee, Y. H., Oblad, P. F. & Peters, J. C. Dinitrogen complexes supported by tris(phosphino)silyl ligands. *Inorg. Chem.* **48**, 2507–2517 (2009).
51. Del Castillo, T. J., Thompson, N. B. & Peters, J. C. A synthetic single-site Fe nitrogenase: high turnover, freeze-fuench ^{57}Fe Mössbauer data, and a hydride resting state. *J. Am. Chem. Soc.* **138**, 5341–5350 (2016).
52. Brown, T. J., Weber, D., Gagné, M. R. & Widenhoefer, R. A. Mechanistic analysis of gold(I)-catalyzed intramolecular allene hydroalkoxylation reveals an off-cycle bis(gold) vinyl species and reversible C–O bond formation. *J. Am. Chem. Soc.* **134**, 9134–9137 (2012).
53. Suryanto, B. H. R. *et al.* Nitrogen reduction to ammonia at high efficiency and rates based on a phosphonium proton shuttle. *Science* **372**, 1187 (2021).
54. Hodgetts, R. Y. *et al.* Refining universal procedures for ammonium quantification via rapid ^{1}H NMR analysis for dinitrogen reduction studies. *ACS Energy Lett.* **5**, 736–741 (2020).
55. Macpherson, J. V. A practical guide to using boron doped diamond in electrochemical research. *Phys. Chem. Chem. Phys.* **17**, 2935–2949 (2015).
56. Nielander, A. C. *et al.* A versatile method for ammonia detection in a range of relevant electrolytes via direct nuclear magnetic resonance techniques. *ACS Catal.* **9**, 5797–5802 (2019).

Acknowledgments: We thank the Dow Next Generation Educator Funds and Instrumentation Grants for their support of the NMR facility at Caltech. We also thank the Resnick Water and Environment Laboratory at Caltech for the use of their instrumentation. We thank the following

533 funding agencies: Department of Energy, Office of Basic Energy Sciences (DOE-0235032),
534 Catalysis Science Program (for the development and applications of CPET mediators); National
535 Institutes of Health (R01 GM-075757) (for studies of Fe-mediated N_2RR). P.G.B. thanks the
536 Ramón Areces Foundation for a postdoctoral fellowship. J.D. thanks the Arnold and Mabel
537 Beckman Foundation for a postdoctoral fellowship. M.J.C. thanks the Resnick Sustainability
538 Institute for a graduate fellowship.

539 **Author contributions:** P.G.B., M.J.C. and J.C.P. conceptualized the work. P.G.B. designed and
540 executed the experiments. J.D. assisted with the execution of the catalytic experiments. All authors
541 analyzed, interpreted the data and cowrote the manuscript.

542 **Competing interests:** The authors declare no competing interests.

543 **Materials & Correspondence:** should be addressed to J.C.P.

544 **Supplementary information:** This file contains Supplementary Text and Data, Supplementary
545 Table S1, and Supplementary Figures S1-S85 - see contents page for details**.**

546

Supplementary Files

This is a list of supplementary files associated with this preprint. Click to download.

- TandemN2SIFinal.docx